Investigation of the SQUBIC phase mask design for depth-invariant widefield microscopy point-spread function engineering

Ana Doblas[a], Sharon V. King[b], Nurmohammed Patwary[b], Genaro Saavedra[a], Manuel Martínez-Corral[a], Chrysanthe Preza*[b]

[a]Dept. of Optics, Univ. of Valencia, E-46100, Burjassot, Spain; [b]Dept. of Electrical and Computer Engineering, Univ. of Memphis, Memphis, TN, USA

ABSTRACT

Point-spread function engineering (PSF), achieved by placing a phase mask at the pupil plane of the imaging lens to encode the wavefront emerging from an imaging system, can be employed to reduce the impact of spherical aberration (SA) in 3D microscopy. In a previous study, the effect of SA on a confocal scanning microscope using a squared cubic phase mask (SQUBIC) was investigated using computer simulations. Here the effect of the SQUBIC design parameter on the insensitivity of the engineered PSF to SA is investigated using a metric based on the second-order moment of the axial variability of the PSF. We show that it is possible to find the optimum SQUBIC for the insensitization to SA.

Keywords: Point-spread function engineering, wavefront coding, spherical aberration

1. INTRODUCTION

In any real widefield high NA optical microscope used for observing biological samples, the PSF varies as a function of depth from the coverslip. The dominant factor causing this variation is the depth-dependent spherical aberration (SA) resulting from the mismatch between the refractive indices of mounting and immersion mediums [1, 2]. The SA impact becomes greater when focusing deeper into the specimen, degrading the image and imposing a practical limit on the sample thickness. Widefield microscopy is a standard tool for studying biological specimens, thus this limitation has driven the development of different methodologies to overcome the SA distortion. Methods based on the modification of the tube length at which the microscope objective (MO) operates [3-5], the use of a collection collar [6], the wavefront coding (WFC) technique [7-16] and adaptive optics [17-20] are among the most used. Although the most accurate compensation is achieved by using adaptive optics, WFC is the most used due to its relative simplicity and potentially inexpensive experimental implementation. WFC is a hybrid procedure in which, first, the PSF of the optical system is modified by a phase mask which produces a new PSF that is insensitive to SA. This invariable PSF allows, in the second stage, the application of deconvolution algorithms to obtain a 3D image free of SA distortion.

In order to enable PSF engineering that addresses the impact of SA, we describe a procedure for design selection that is directly associated with the axial-PSF variability as a function of SA. The merit function used is based on the calculation of the width of the axial intensity distribution, which depends on the SA induced in the focusing process [21]. This merit function is used to guide the selection of the scaling parameter in a squared cubic phase mask (SQUBIC).

In this paper, we first present the mathematical expression of the PSF obtained in a high NA system. Numerical simulations are shown to demonstrate the depth-variability induced during the focusing process. Section 3 presents the strategy to determine the optimal design for compensation of the effect of the SA. In this section, we also select a suitable phase mask design of SQUBIC, previously studied in confocal microscopy [16], and evaluate PSF variability for different design parameters. Simulated SQUBIC-PSFs are presented in Section 4 to demonstrate the effectiveness of our design. The main achievements of this study are summarized in Section 5.

*cpreza@memphis.edu; phone (901) 678-4369; fax (901) 678-5469; cirl.memphis.edu

Three-Dimensional and Multidimensional Microscopy: Image Acquisition and Processing XXI, edited by Thomas G. Brown, Carol J. Cogswell, Tony Wilson, Proc. of SPIE Vol. 8949, 894914

doi: 10.1117/12.2038610

2. SPHERICAL ABERRATION INDUCED IN FLUORESCENCE MICROSCOPY

In order to describe the effect of SA, we first consider the 3D amplitude PSF in a fluorescence microscope. High-resolution microscopy is achieved with the use of high numerical aperture (NA) objective lenses. In this case, the PSF cannot be calculated by means of paraxial diffraction formulas and therefore, must be calculated through the non-paraxial Debye's formulation [22].

According to this, and assuming that the sine condition [23, 24] and axial symmetry hold, the amplitude PSF is given by

$$h\left(r_N, z_N\right) = \int_0^{\alpha} p\left(\theta\right)\sqrt{\cos\theta}J_0\left(2\pi r_N \frac{\sin\theta}{\sin\alpha}\right)\exp\left[i2\pi W\left(\theta\right)\right]\exp\left[-i2\pi z_N \frac{\sin^2(\theta/2)}{\sin^2(\alpha/2)}\right]\sin\theta\,\mathrm{d}\theta, \tag{1}$$

where the lateral and axial normalized coordinates, (r_N, z_N), are related to the regular coordinates, (r, z), as

$$r_N = \frac{n}{\lambda} r \sin\alpha\ , \quad z_N = \frac{2n}{\lambda} z \sin^2\left(\alpha/2\right), \tag{2}$$

being α the maximum value for the aperture angle θ, n the refractive index of the immersion medium, and λ the emission wavelength. The computation of Equation (1) requires knowledge of the complex transmittance at the aperture stop of the optical imaging system, $p(\theta)$. The phase factor $W(\theta)$ in Equation (1) represents the potential phase distortions produced in the focusing process.

As shown in [16], the expression of $W(\theta)$ as a function of both the refractive defocus parameter, w_{20}, and the primary SA parameter, w_{40}, is given by

$$W\left(\theta; z_s\right) = w_{20}\left(z_s\right)\frac{\sin^2(\theta/2)}{\sin^2(\alpha/2)} + w_{40}\left(z_s\right)\frac{\sin^4(\theta/2)}{\sin^4(\alpha/2)}. \tag{3}$$

It is worth noting that both the refractive defocus and the primary SA coefficients depend on the axial scanning depth, z_s , which is the scanning distance where the source is located without aberration, and their expressions can be expressed as

$$w_{20}\left(z_s\right) = \frac{2n}{n'}\left(n' - n\right)\sin^2\left(\frac{\alpha}{2}\right)\frac{z_s}{\lambda}, \tag{4}$$

and

$$w_{40}\left(z_s\right) = \frac{n}{n'^3}\left(n'^2 - n^2\right)\sin^4\left(\frac{\alpha}{2}\right)\frac{z_s}{\lambda}, \tag{5}$$

where n' is the refractive index of the medium in which the specimen is embedded. As stated above, a minimum mismatch between refractive indices of the sample medium and the immersion liquid induces a significant amount of SA.

After inserting Equation (3) into Equation (1) and defining a reduced axial coordinate as $z_N' = z_N - w_{20}$, we obtain the following expression for the 3D amplitude PSF

$$h\left(r_N, z_N'\right) = \int_0^{\alpha} p\left(\theta\right)\sqrt{\cos\theta}J_0\left(2\pi r_N \frac{\sin\theta}{\sin\alpha}\right)\exp\left[i2\pi w_{40}\frac{\sin^4(\theta/2)}{\sin^4(\theta/2)}\right]\exp\left[-i2\pi z_Z' \frac{\sin^2(\theta/2)}{\sin^2(\alpha/2)}\right]\sin\theta\,\mathrm{d}\theta. \tag{6}$$

Equation (6) allows for computation of a numerical 3D PSF in which the induced SA can be easily taken into account. The numerical computation of these equations is available via the PSF computation module of the Computational Optical Sectioning Microscopy Open Source (COSMOS) software package [25]. The PSF computation mode uses the Gibson and Lanni PSF model [1]. In Figure 1 we show the results of this computation for a conventional (circular clear pupil, CCA) fluorescence microscope equipped with a dry objective lens (20×/0.8 NA) and a light point source ($\lambda = 515$

nm), which is embedded in water ($n' = 1.33$), and located at varying depths, z_s, below the coverslip. PSFs are computed on a 128×128×1024 grid with cubic voxels of 0.1μm. From Figure 1 it is trivial to realize that the axial response of a conventional imaging system depends on SA. This demonstrates the need to investigate and select pupil mask parameters that could reduce the SA impact on WFC-PSFs.

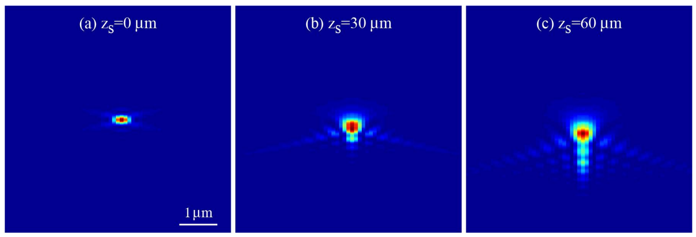

Figure 1. Depth variant axial response of the conventional PSF. XZ views of the conventional PSF for focusing depth z_s: (a) z_s = 0 μm; (b) z_s = 30 μm and (c) z_s = 60 μm.

3. DESIGN OF PHASE FILTERS FOR REDUCING SA IMPACT

Our aim in this study is the design of a phase mask for reducing the SA impact in the focusing process of the imaging system. Although this effect should be studied throughout a 3D function, our metric quantifies the sensitivity to SA by measuring the change of the axial intensity distribution of the imaging system. The goal for the selection of a phase mask is to identify one that produces the most invariant axial response for varying amounts of SA.

To fix our attention in the axial behavior, we must particularize Equation (6) for points located at the optical axis ($r_N = 0$) and therefore we introduce the following non-linear mapping variable [8-10, 16]

$$\zeta = \frac{\sin^2(\theta/2)}{\sin^2(\alpha/2)} - \frac{1}{2} \tag{7}$$

Taking into account this transformation and assuming $q(\zeta) = p(\theta)\sqrt{\cos\theta}$, Equation (6) becomes

$$h\left(w_{20}', w_{40}\right) = \int_{-0.5}^{0.5} q\left(\zeta\right) \exp\left[i2\pi w_{40}\zeta^2\right] \exp\left[-i2\pi w_{20}'\zeta\right] \mathrm{d}\zeta, \tag{8}$$

where $w_{20}' = z_N' - w_{40}$ is the reduced defocus coefficient. Equation (8) establishes a Fourier-transform relationship between the axial amplitude response of the system and the mapped pupil function $q(\zeta)$ when no SA is induced. Note that for a CCA its corresponding mapped pupil function is $q_{CCA}(\zeta) = \mathrm{rect}(\zeta)$. It is clear that the presence of SA, accounted for by the w_{40} coefficient, can be understood as a modification of the effective pupil of the system $q(\zeta; w_{40}) = q(\zeta)\exp(i2\pi w_{40}\zeta^2)$.

The formula in Equation (8) is similar to the one obtained in the analysis of 1D paraxial focusing system when considering a cylindrical lens illuminated by a monochromatic plane wave. In this case, as stated in [16], the 1D defocus coefficient plays a role similar to the one played by the coefficient w_{40} in Equation (8). It is clear that the solutions obtained for increasing the depth of field in the 1D case [26] can also be applied to decrease the sensitivity of the axial response to depth-induced SA in a high-NA imaging system.

Adapting these ideas for solving the problem of SA impact reduction, we use a pupil phase mask, that we called SQUBIC mask, which was previously reported in [16], whose mapped transmittance is given by

$$q(\zeta) = rect(\zeta)\exp\left[i2\pi A\zeta^3\right]. \tag{9}$$

As stated above, the value of *A* is set taking into account the slowest evolution of the variance of the axial intensity distribution. Following [21], the width of a function can be assessed by means of its variance, given by

$$\sigma^2_{w'_{20}}\left(w_{40}\right) = \left\langle w'^{2}_{20}\right\rangle_{w_{40}} - \left\langle w'^{1}_{20}\right\rangle^2_{w_{40}}, \tag{10}$$

where

$$\left\langle w'^{n}_{20}\right\rangle_{w_{40}} = \frac{1}{\left(-i2\pi\right)^n}\int_{-\infty}^{+\infty}\frac{\mathrm{d}^n q\left(\zeta;w_{40}\right)}{\mathrm{d}\zeta}q^*\left(\zeta;w_{40}\right)\mathrm{d}\zeta. \tag{11}$$

Note that in Equation (10) the expression of $< w'^{2}_{20} >$ is obtained in terms of the Fourier transform of $h\left(w'_{20};w_{40}\right)$ and its corresponding derivatives.

For the case of a SQUBIC mask, we calculate now the moments in Equation (10) up to second order. It is worth noting that in this case the second-order moment of the axial irradiance response diverges because the system contains hard-edge diffraction elements. This problem is overcome using a generalized second-order moment as shown in [21]. The final expression of the variance of the axial distribution is

$$\sigma^2_{w'_{20}}\left(w_{40}\right) = \frac{4}{\pi^2} + \frac{A^2}{20} + \frac{w^2_{40}}{3}, \tag{12}$$

From Equation (11) one can denote that the evolution of the width for SQUBIC design follows a parabola whose minimum is located at $w_{40} = 0$. It is worth to note that the slower the variation of this width, the more tolerant the system is to SA. As a merit function to estimate this variation we use the normalized variance

$$\sigma^2_{norm}\left(w_{40}\right) = \frac{\sigma^2_{w'_{20}}\left(w_{40}\right)}{\sigma^2_{w'_{20}}\left(0\right)} = 1 + \Gamma w^2_{40}, \tag{13}$$

being

$$\Gamma = \frac{20\pi^2}{240 + 3\pi^2 A^2}. \tag{14}$$

The variation of this parameter, Γ, as a function of the SA parameter is shown in Figure 2. Note that the higher the value of *A* in the SQUBIC design, the slower the variation of this function with SA. Note also the greatly improved performance of the SQUBIC system in comparison with the conventional system in terms of its sensitivity to SA.

Although Equation (13) dictates that the higher the value of *A* the slower the variability of the system with the SA, it exists an upper limit of this value due to practical implementation restrictions. As Figure 3 illustrates, the values of the phase map change rapidly towards the extreme of the SQUBIC design. Furthermore, this variation becomes higher with the rise of the value of *A*. Any real implementation of this masks (lithography or spatial light modulators, for example) presents an experimental constraint in the proper display of the phase design. Thus, the SQUBIC optimum design parameter will be identified as the maximum value of *A* which provides a correct sampling of the phase of the mask by using the actual implementation technique.

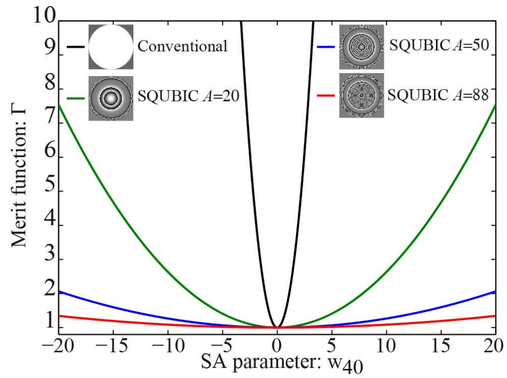

Figure 2. Evolution of the merit function, Γ, for the conventional system and for SQUBIC designs with varying *A* parameter. The phase wrapped maps, from 0 to 2π, for each phase mask design are also shown.

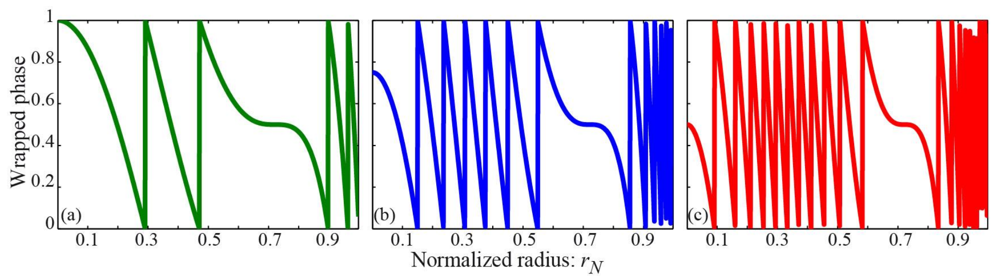

Figure 3. Wrapped phase values along the normalized radius for different SQUBIC designs: (a) *A*=20, (b) *A*=50 and (c) *A*=88.

4. SIMULATED SQUBIC-PSF IMAGES

Simulated SQUBIC and CCA PSFs are computed to validate our metric of sensitivity to SA. Toward this end, the COSMOS software [25] was used to compute these results. Here, SQUBIC-PSFs are simulated for three design parameters: *A* = 20, 50 and 88. Figure 4 shows XZ views of these SQUBIC PSFs obtained with different amount of SA. Clearly, the XZ irradiance distributions seem more insensitive to the focusing depth in comparison to Figure 1.

However, from Figure 4 it is difficult to investigate the effect of the parameter *A* on the variability of the SQUBIC PSF as a function SA. The influence of the design parameter can be clearly shown if one plots the axial intensity distribution of Figure 4. Next, in Figure 5 we show the profile of the axial intensity distribution in the focal spot for each focusing depth. This demonstrates the great performance advantage in axial sensitivity to SA achieved with SQUBIC implementation. These profiles show that the selected SQUBIC design (*A* = 88) achieves the most invariant system in the presence of SA, as predicted by the variance metric.

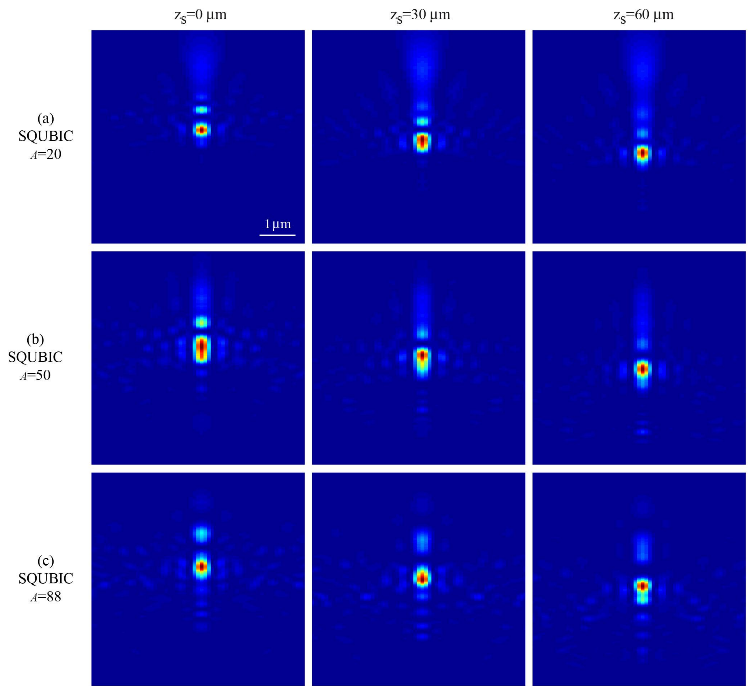

Figure 4. Depth invariant axial response of the SQUBIC PSF; XZ view of SQUBIC-PSFs for a 20x/0.8NA air-immersion lens using different design parameter and with different amount of SA.

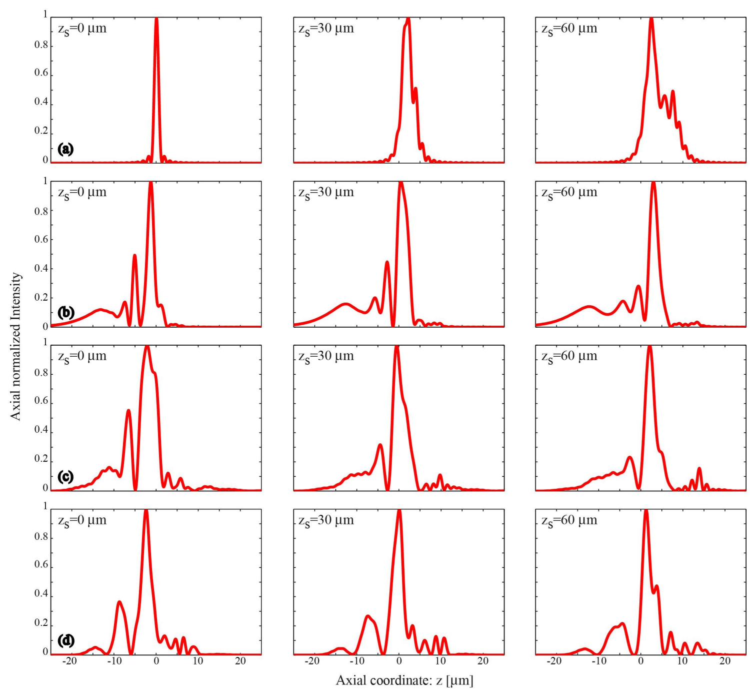

Figure 5. Axial intensity distribution profiles of PSFs in Figure 1 and 3; for increasing (left to right) amounts of the scanning depth, z_s: (a) CCA; (b) SQUBIC with A=20; (c) SQUBIC with A=50; and (d) SQUBIC with A=88.

5. CONCLUSIONS

The use of the WFC technique to improve the insensitivity of fluorescence microscopy to SA has been shown previously. However, in this paper we introduce the variance as a metric to find the optimal design parameter that maximizes the SA tolerance. This analysis provides a powerful, simple mathematical tool to tackle the design strategies for compensation of the effect of the SA on the system response. The method is based on the calculation of the normalized variance of the axial response of the imaging system. The goal is to achieve a design with constant behavior of the variance values for varying amount of SA. Using this technique, the performance of the family of SQUBIC masks has been analyzed and investigated for varying design parameters. Numerical simulations show that the higher the value of the SQUBIC design parameter the more invariant the WFC system PSF is to SA.

ACKNOWLEDGMENTS

Financial support by the Ministerio de Economia y Competitividad, Spain (Grant DPI2012-32994), the Generalitat Valenciana (Grant PROMETEO2009-077) and the National Science Foundation Career Award DBI-0844682 (P.I: C. Preza) is gratefully acknowledged. A. Doblas greets funding from the University of Valencia through the predoctoral Fellowship Program “Atracció de Talent”.

REFERENCES

[1] Gibson, S. F. and Lanni, F., "Experimental Test of an Analytical Model of Aberration in an Oil-Immersion Objective Lens Used in 3-Dimensional Light-Microscopy," Journal of the Optical Society of America A 9(1), 154-166 (1992).

[2] Török, P., Varga, P. and Nemeth, G., "Analytical solution of the diffraction integrals and interpretation of wave-front distortion when light is focused through a planar interface between materials of mismatched refractive indices," Journal of the Optical Society of America A 12(12), 2660-2671 (1995).

[3] Sheppard, C. J. R. and Gu, M., “Aberration compensation in confocal microscopy,” Applied Optics 30(25), 3563-3568 (1991).

[4] Ke, P. C. and Gu, M., “Characterization of trapping force in the presence of spherical aberration,” Journal of Modern Optics 45(10), 2159-2168 (1998).

[5] Reihani, S. N. S., Khalesifard, H. R. and Golestanian, R., “Measuring lateral efficiency of optical traps: the effect of tube length,” Optics Communications 259(1), 204–211 (2006).

[6] Schwertner, M., Booth, M. J. and Wilson, T., “Simple optimization procedure for objective lens correction collar setting,” Journal of Microscopy 217(3), 184–187 (2005).

[7] Mills, J. P. and Thompson, B. J., “Effect of aberrations and apodization on the performance of coherent optical systems. I. The amplitude impulse response,” Journal of the Optical Sociecty of America A 3(5), 694–703 (1986).

[8] Ojeda-Castañeda, J., Andrés, P. and Diaz, A., “Annular apodizers for low sensitivity to defocus and to spherical aberration,” Optics Letters 11(8), 487–489 (1986).

[9] Ojeda-Castañeda, J., Andrés, P. and Diaz, A., “Strehl ratio with low sensitivity to spherical aberration,” Journal of the Optical Society of America A 5(8), 1233–1236 (1988).

[10] Ojeda-Castañeda, J., Tepichin, E. and Pons, A., “Apodization of annular apertures: Strehl ratio,” Applied Optics 27(24), 5140–5145 (1988).

[11] Mezouari S. and Harvey, A. R., “Phase pupil functions for reduction of defocus and spherical aberration,” Optics Letters 28(10), 771–773 (2003).

[12] Carles, G., Carnicer, A. and Bosch, S., “Phase mask selection in wavefront coding systems: A design approach,” Optics and Lasers in Engineering 48(7), 779-785 (2010).

[13] Vettenburg, T., Bustin, N. and Harvey, A. R., “Fidelity optimization for aberration-tolerant hybrid imaging systems,” Optics Express 18(9), 9220-9228 (2010).

[14] Yuan, S. and Preza, C., "Point-spread function engineering to reduce the impact of spherical aberration on 3D computational fluorescence microscopy imaging," Optics Express 19(23), 23298-23314 (2011).

[15] Arnison, M. R., Cogswell, C. J., Sheppard, C. J. R. and Török, P., [Wavefront coding fluorescence microscopy using high aperture lenses], Springer-Verlag, Berlin, 143-165 (2003).

[16] Saavedra, G., Escobar, I., Martinez-Cuenca, R., Sánchez-Ortiga, E. and Martínez-Corral, M., "Reduction of spherical-aberration impact in microscopy by wavefront coding," Optics Express 17(16), 13810–13818 (2009).
[17] Booth, M. J., Neil, M. A. A., Juskaitis, R. and Wilson, T., "Adaptive aberration correction in a confocal microscope," Proceedings of the National Academy of Sciences U.S.A. 99(9), 5788–5792 (2002).
[18] Theofanidou, E., Wilson, L., Hossak, W. J. and Artl, J., "Spherical aberration correction for optical tweezers," Optics Commununications 236(1), 145–150 (2004).
[19] Somalinga, S., Dressbach, K., Hain, M., Stankovic, S., Tschudi, T., Knittel, J. and Richter, H., "Effective spherical aberration compensation by use of nematic liquid-crystal device," Applied Optics 43(13), 2722–2729 (2004).
[20] Booth, M. J., "Adaptative optics in microscopy," Philosophical Transactions of the Royal Society A 365(1861), 2829-2843 (2007).
[21] Escobar, I., Sánchez-Ortiga, E., Saavedra, G. and Martínez-Corral, M., [New analytical tools for evaluation of spherical aberration in optical microscopy], Springer-Verlag, Berlin, 85-99 (2011).
[22] Debye, P., "Light near a focal point or line," Annalen der Physik 30, 755-776 (1909).
[23] M. Born and E. Wolf, Principles of Optics (Pergamon, New York, 1980).
[24] Sheppard, C. J. R. and Matthews, H. J., "Imaging in high-aperture optical system," Journal of the Optical Society of America A 4(8), 1354-1360 (1987).
[25] "Computational Imaging Research Laboratory, Computational Optical Sectioning Microscopy Open Source (COSMOS) software package ", retrieved http://cirl.memphis.edu/COSMOS.
[26] Dowski, E. R. and Cathey, W. T., "Extended depth of field through wave-front coding," Applied Optics 34(11), 1859-1866 (1995).